Radiation Physics and Chemistry 166 (2020) 108473

Contents lists available at ScienceDirect

Radiation Physics and Chemistry

journal homepage: www.elsevier.com/locate/radphyschem

2D dose reconstruction of IMRT patient-specific QA based on log file

Sayid Mubarok[a,c], Wibowo Edy Wahyu[b], Pawiro Ardjo Supriyanto[a,*]

[a] Department of Physics, Faculty of Mathematics and Natural Sciences, Universitas Indonesia, Depok, 16424, West Java, Indonesia
[b] Department of Radiotherapy, Cipto Mangunkusumo Hospital, Jakarta, Indonesia
[c] Department of Radiology, Fatmawati Hospital, Jakarta, Indonesia

ARTICLE INFO

Keywords:
Log files
Dose reconstruction
Patient-specific QA
IMRT
Gamma evaluation

ABSTRACT

This study aims to reconstruct the 2D dose distribution based on log file and use it for IMRT patient-specific QA. Log files retrieved from Varian Unique Linear Accelerator was extracted to calculate the MU fluence and converted into 2D dose distribution using the modified Clarkson integration (MCI) method. All calculations were performed using the MATLAB scripts and functions. This reconstruction assumed that the cube water phantom was irradiated by 6 MV photon at source surface distance (SSD) 98.5 cm and at depth of 1.5 cm. This 2D dose reconstruction was compared with EclipseTM treatment planning system (TPS) calculation. The evaluation was done based on isocenter point and 2D gamma index analysis. The evaluation was separated by the split field (large IMRT field) and non-split field (small IMRT field). The isocenter dose evaluation results were 89% and 36% of data for non-split field and split field had deviation under 3%. The gamma pass-rate results for non-split field with 2%/2 mm, 3%/3 mm and 4%/4 mm criteria were above 84%, 90% and 95%. On the other hand, the gamma pass-rate results for split field with 2%/2 mm, 3%/3 mm and 4%/4 mm criteria were above 78%, 85% and 90%. These results show that log file information can be used to reconstruct 2D dose distribution and potentially to be used for IMRT patient-specific QA.

1. Introduction

The purpose of intensity-modulated radiation therapy (IMRT) patient-specific QA is to ensure that the actual radiation delivery parameters correspond to the planned radiation parameters generated from Treatment Planning System (TPS). IMRT patient-specific QA should be efficient, automatic and applicable to ensure the safety of patient treatment. Linear accelerator (LINAC) can generate the log file that can be employed to evaluate the radiation accuracy for pre-and-post-treatments delivered to the specific patient. Varian LINAC log files create information about multileaf collimator (MLC), jaws position, carriage position, gantry position and MU fraction generated every 50 m. The log files data usually were used to verify the MLC speed or position for IMRT and volumetric-modulated arc therapy (VMAT) techniques (LoSasso, 2008; McGarry et al., 2016; Midi and Zin, 2017; Rangaraj et al., 2013). The data from the log files is a potential information to reconstruct dose not only in phantom but also in patient (Osewski et al., 2014). The Varian log files can also be used to reconstruct the dose volume histogram (DVH) if the log files information is combined with CT patient data and treatment planning system (Jf, 2014; Osewski et al., 2014; Tae-Suk et al., 2009). The log files also can be used to calculate and verify the 3D dose delivered using the Mobius FX for IMRT and VMAT techniques (Vazquez-Quino et al., 2017).

Kung et al. (2000) introduced a method for MU verification calculation in IMRT technique based on the concept of modified Clarkson integration (MCI). Xing et al. (2000) used the modified Clarkson integration with simple scatter-summation algorithm. Meanwhile, Yang et al. (2003) used the modified Clarkson integration with the inclusion of head scatter and MLC transmission for IMRT technique. All these methods were designed for step-and-shoot IMRT technique. Chen et al. (2005) developed an MU verification calculation for sliding window IMRT using the dynamic MLC (DMLC) files that were generated by the IMRT treatment planning system. All evaluations of this study compare some points of calculation dose based on the developed method with the calculation of a commercial treatment planning system.

This study aims to reconstruct the 2D dose distribution for sliding window IMRT using the modified Clarkson Integration based on log files generated from linear accelerator after patient irradiation or after IMRT QA irradiation. The evaluation of this study does not only compare the point dose, but also the 2D dose based on gamma index evaluation.

* Corresponding author.
E-mail address: supriyanto.p@sci.ui.ac.id (P.A. Supriyanto).

https://doi.org/10.1016/j.radphyschem.2019.108473
Received 31 May 2019; Accepted 31 August 2019
Available online 06 September 2019
0969-806X/

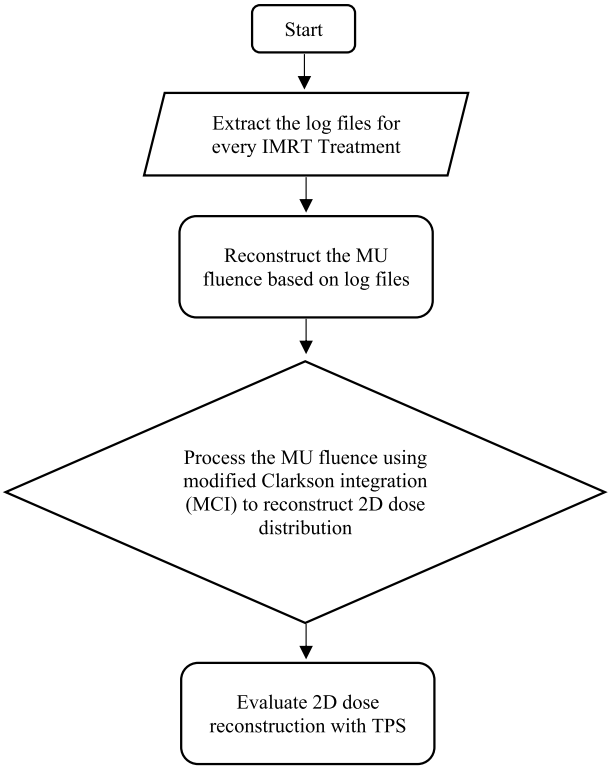

Fig. 1. Flow chart to reconstruct the 2D dose distribution based on log files.

2. Methods

This study was conducted at Cipto Mangunkusomo Hospital, Jakarta, Indonesia, and utilized the log files information generated from the Unique Varian Linear Accelerator (LINAC) 6 MV that was manufactured in China. The LINAC has 120 MLC divided into 60 MLC(s) at both of Bank A and Bank B. The procedure to reconstruct 2D dose distribution from log files is summarized in a flow chart as shown in Fig. 1.

2.1. Extracting the log files

On the default mode, the log files are not saved automatically on the system such that certain commands at VxWork® application are required to configure the system to save and generate the log file automatically after the irradiation of IMRT field. The two files with.dlg extension will be saved on some directory (usually at D:\VMSOS \AppData\MLC\Controller\MLCDynalogs). Those files contain the MLC information for Bank A and Bank B. Dynalog file viewer reference guide document is used as a protocol to generate the log files from Varian LINAC system (DynaLog File Viewer Reference Guide, 2015).

2.2. MU fluence reconstruction based on log file information

The log files comprise the information about MU fraction, jaw position, and MLC position captured every 50 ms. This information was used to reconstruct the MU fluence. A MATLAB script and function have been built to reconstruct the MU fluence. A blank array which represents 40 cm × 40 cm field was prepared. This array has 2 mm pixel resolution and the pixel value for every segment of IMRT field depends on the pixel location (the pixel location at the open field, blocked by the MLC or blocked by the jaws). The array pixels unblocked by the MLC and jaws have the same pixel value as the MU fraction (Mubarok et al., 2019). Additionally, the array pixels unblocked by jaws but blocked by MLC have the pixel value 2% of the MU fraction (the MLC transmission was assumed 2%) (Khan, 2014; LoSasso et al., 1998; Mubarok et al., 2019). On the other hand, the array pixels blocked by jaws and MLC have the zero value. The MLC leaves were opened 1 mm bigger than geometrical position because the radiation field offset (RFO) was assumed 1 mm (the measurement of RFO was reported having the value range of 0.5 mm–1.3 mm) (Mubarok et al., 2019; Vial et al., 2006). The MU fluence was reconstructed and summed every 50 ms at all segments of IMRT field irradiation. The illustration to reconstruct the MU fluence can be seen in Fig. 2 and Fig. 3.

2.3. 2D dose reconstruction using Modified Clarkson Integration

2D dose reconstruction based on MU fluence was performed using the modified Clarkson integration (MCI) method. The dose distribution consists of the contribution of primary dose D_p and secondary dose D_s. The MU fluence at cartesian coordinate (x,y) was converted to the circle

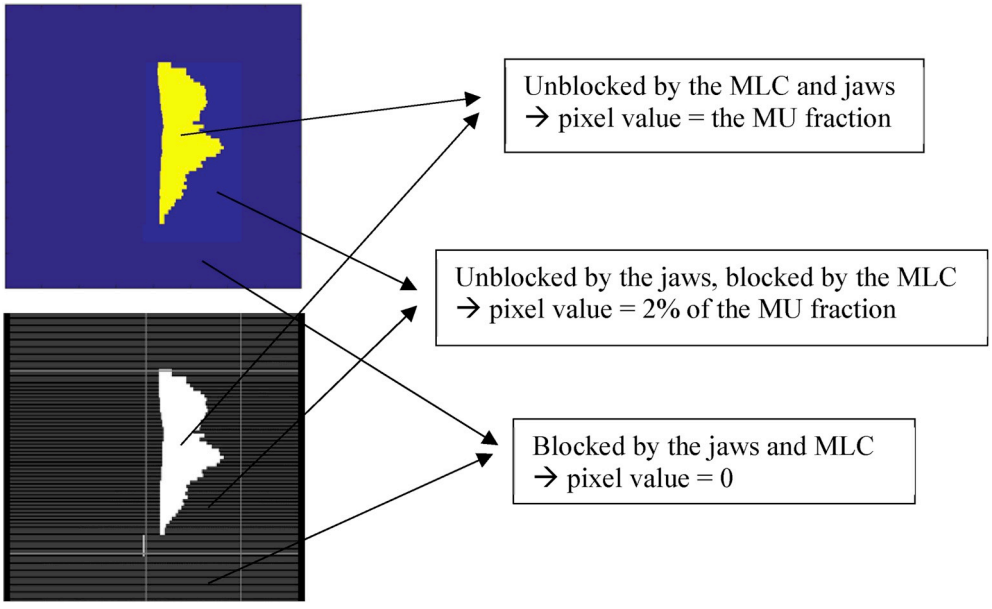

Fig. 2. The pixel value for every segment of IMRT field depends on the pixel location.

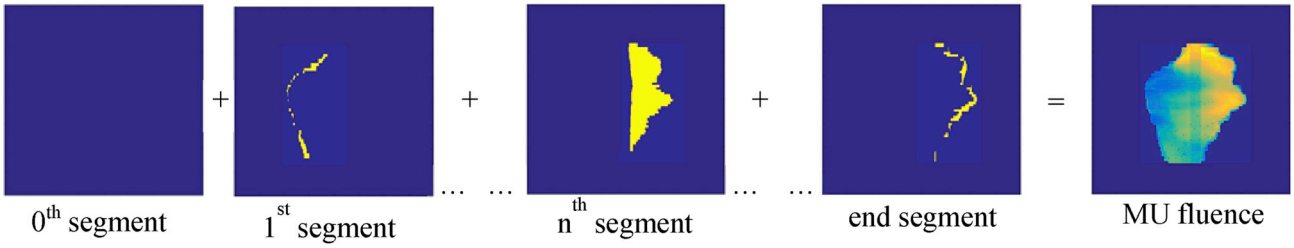

Fig. 3. The illustration to reconstruct the MU fluence. The MU fluence were reconstructed and summed every 50 ms at all segments of IMRT field irradiation.

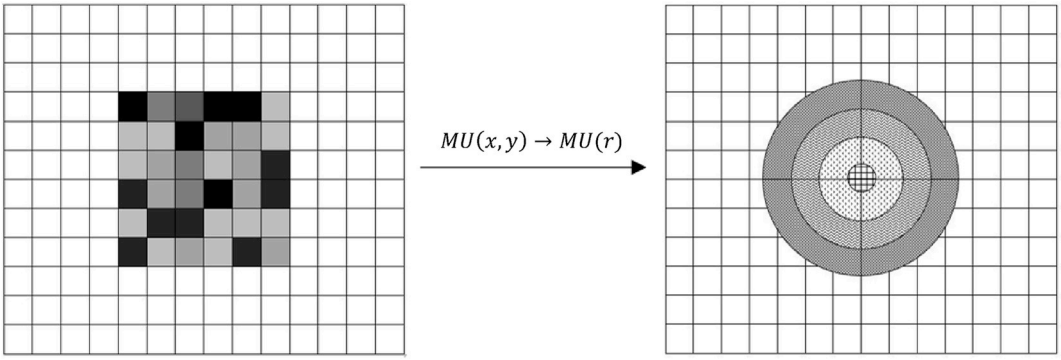

Fig. 4. MU fluence at cartesian coordinate (*x*,*y*) was converted to the circle coordinate (r).

coordinate (r) because there is a symmetry scattering contribution from the pixel in the same radius (see Fig. 4) (Kung et al., 2000; Yang et al., 2003).

$$MU(x, y) \rightarrow MU(r) \equiv \frac{1}{2\pi} \int_{circle} MU(x, y) d\theta \tag{1}$$

The dose equation for each pixel is:

$$D(x, y, z) = MU\left[D_p(x, y, z) + \sum D_s(x, y, z)\right] \tag{2}$$

with D_p and D_s can be calculated using the Equations (3) and (4), respectively.

$$D_p(x, y, z) = \left(\frac{100}{100 - z'}\right)^2 C_f \; Sp(0) TMR(d_{eff}, 0) \, OAR(d_{eff}, x, y) \tag{3}$$

$$D_s(x, y, z) = \left(\frac{100}{100 - z'}\right)^2 C_f \left[Sp(r + \Delta r) TMR(d_{eff}, r + \Delta r) - Sp(r) TMR(d_{eff}, r)\right] OAR(d_{eff}, x, y) \tag{4}$$

where C_f is LINAC calibration factor. $Sp(0)$, $TMR(d_{eff}, 0)$ *and* $OAR(d_{eff}, x, y)$ are phantom scatter factor, tissue maximum ratio and off axis ratio for zero field size, respectively. While $Sp(r)$*and* $TMR(r)$ are phantom scatter factor and tissue maximum ratio for field size with radius r.

The assumption to reconstruct the 2D dose distribution based on MCI calculation method used 40 cm × 40 cm × 40 cm cube water phantom. The 2D dose calculation was measured at z_{max} (depth = 1.5 cm) and using source axis distance (SAD) technique (SSD = 98.5 cm). The contribution of primary dose on this study used the circle with the radius r_p = 4 mm and the contribution of secondary dose was calculated for every addition Δr = 4 mm. The 4 mm radius was selected because its size was considered the most ideal for the array with 2 mm resolution.

2.4. Evaluation of 2D dose reconstruction with treatment planning system (TPS)

2D dose reconstruction was evaluated with the calculation of TPS. Dose distribution on TPS verification plan was created using cube water phantom at SSD = 98.5 cm and depth = 1.5 cm (Fig. 5). The evaluation of point dose has been done by comparing the isocenter of 2D dose reconstruction based on log files with the isocenter dose based on TPS calculation. The planar dose evaluation has been done using gamma index criteria. The formulation of gamma index criteria is shown in Equation (5):

$$\gamma_m = \sqrt{\left(\frac{distance}{DTA}\right)^2 + \left(\frac{dose\ different}{\Delta D}\right)^2} \tag{5}$$

with *distance* is a distance from a reference point to calculation point, *dose different* is percentage deviation of between the value of reference point with calculation point, *DTA* is a distance to agreement and ΔD is the percentage deviation that was accepted (Biggs et al., 2001; Jeraj and Robar, 2004). The acceptable gamma passing rate criteria for this study were set 95% for 4%/4 mm, 90% for 3%/3 mm and 85% for 2%, 2 mm.

3. Results and discussion

3.1. MU fluence and 2D dose reconstruction

The results were divided into split IMRT field and non-split IMRT fields. Because of the limited movement of carriage MLC to cover the large area, the IMRT field was split into two or three fields and combined as if they were just one field. The example of MU fluence and 2D dose reconstruction for split IMRT field can be seen in Fig. 6, while the example for non-split IMRT field can be seen in Fig. 7. Dose reconstruction only calculated the pixels that have a non-zero value of MU fluence. Total time needed to reconstruct 2D dose reconstruction for non-split IMRT field was 147s–292s, while for split IMRT field was 479.0s–1210.5s. The dose reconstruction used MATLAB application with a laptop that had specification processor of Intel(R) Core™ i5-3230M CPU @ 2.60 GHz and 4.00 GB RAM.

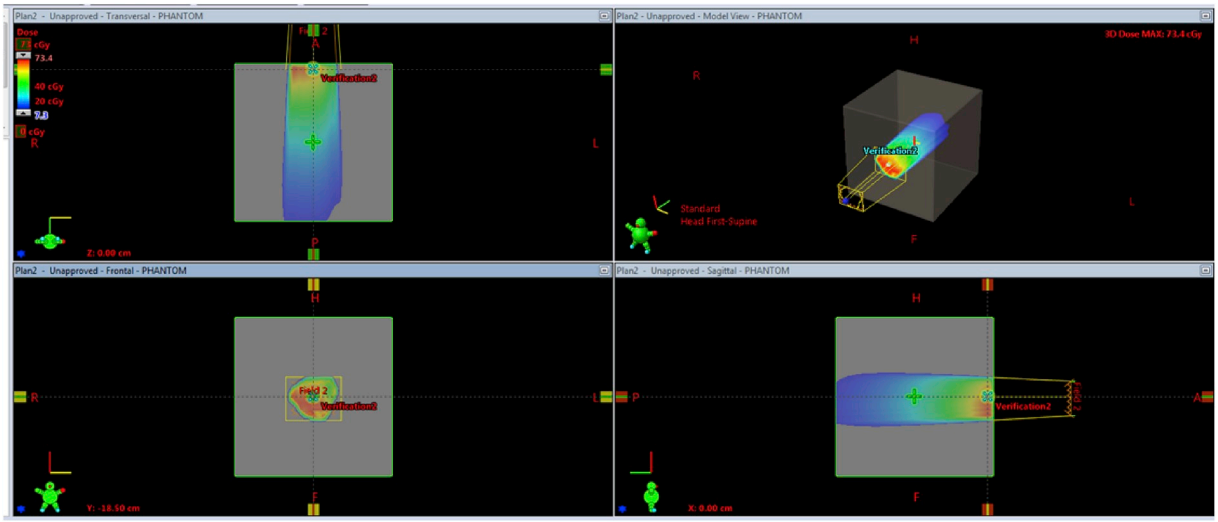

Fig. 5. Verification plan is created on TPS at SSD = 98.5 cm and depth = 1.5 cm.

3.2. Evaluation of 2D dose reconstruction

2D dose reconstruction based on log file information was conducted for 7 cases consisting of 2 brain cases, 2 breast cases, inguinal, cervix and nasopharynx. The evaluation was separated into split IMRT field (large field) and non-split IMRT field (small field). The comparison isocenter dose point between 2D dose reconstruction based on MCI method and TPS calculation can be seen in Fig. 8. Almost all data (89% data) for non-split IMRT field had deviation below 3%. All data that had deviation below 3% showed the isocenter location at the center of the irradiation field (Fig. 9a), but for the data that had deviation above 3% showed the isocenter location at the edge of irradiation field (penumbra region) (Fig. 9b). These results were in line with Kung et al. (2000), Xing et al. (2000) and Yang et al. (2003), the isocenter dose point were between 3% and 5% The results for split IMRT field show that only 36% data had deviation under 3%. This is because the isocenter location for split IMRT field is usually at the junction where the IMRT beam is split and this is in line with Chen et al. (2005), where for large IMRT field, the isocenter dose point can be higher than 10%. The results on the evaluation of isocenter dose point for split IMRT are relatively poor than those results for non-split IMRT field. This corresponds to the disagreement between the MCI method and TPS calculation at the junction where the IMRT beam is split. Fig. 10a and b shows the areas of the mismatched pixels between the MCI method and the TPS calculation. Evaluation based on the 2D dose modification for the MCI method shows inconsistencies with the TPS calculation in the non-split

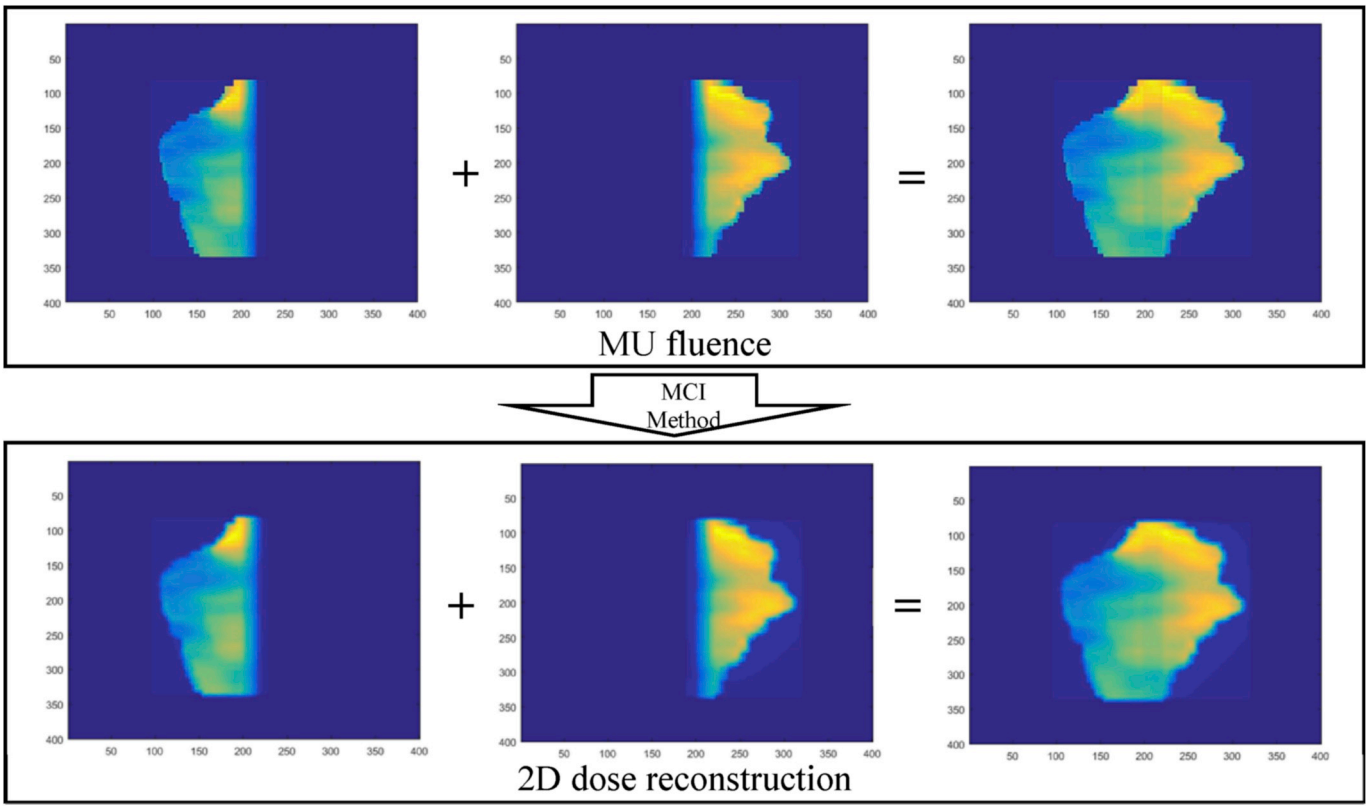

Fig. 6. MU fluence and 2D dose reconstruction for split IMRT field.

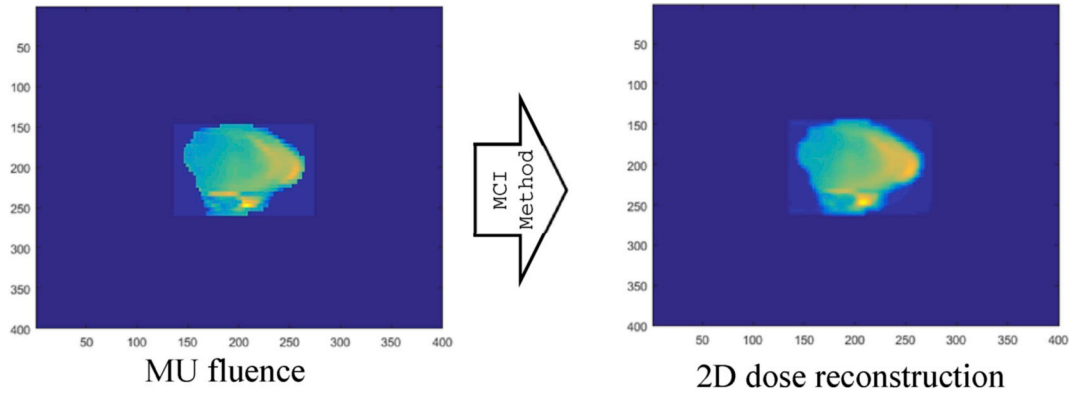

Fig. 7. MU fluence and 2D dose reconstruction for non-split IMRT field.

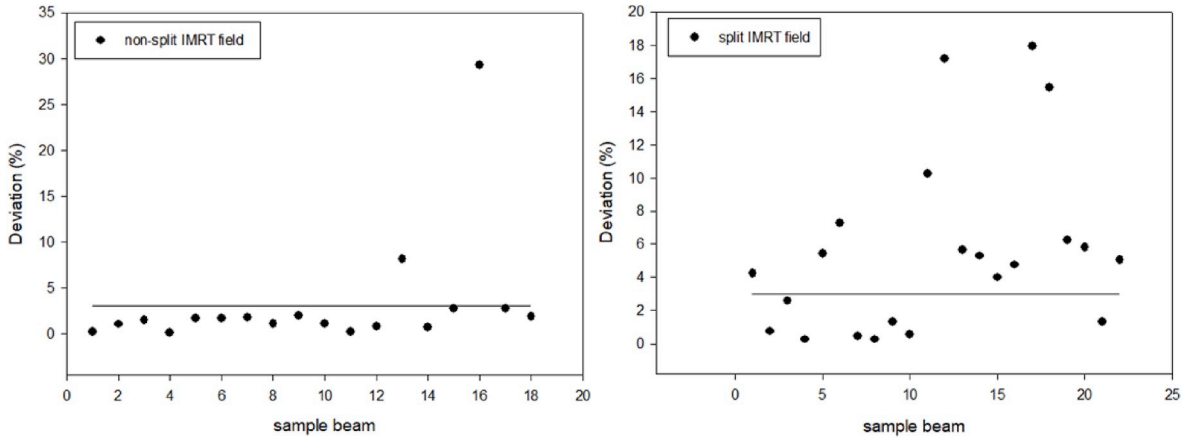

Fig. 8. The deviation isocenter dose point between 2D dose reconstruction based on MCI method and TPS calculation.

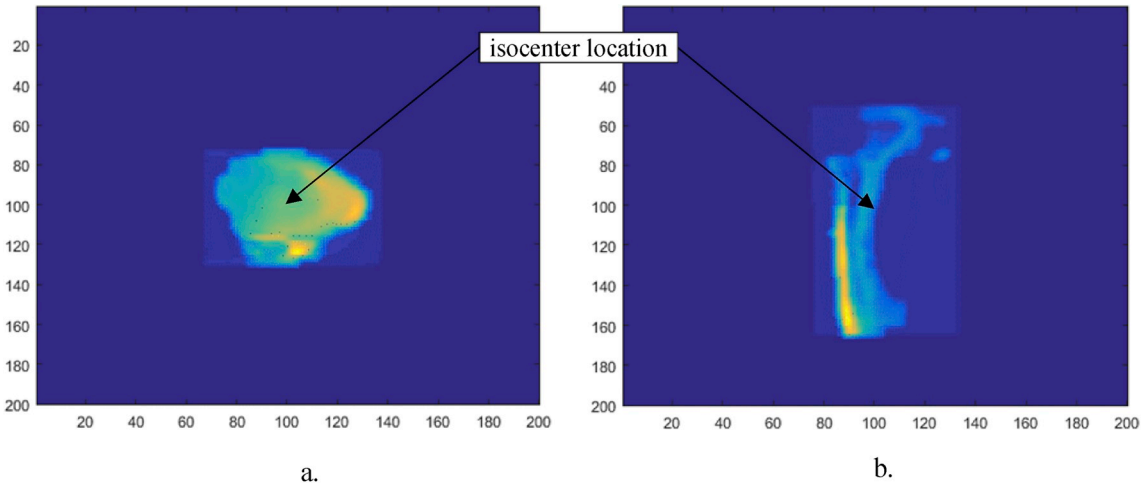

Fig. 9. The example of isocenter location of non-split IMRT field. a. The isocenter location at center of the irradiation field (beam 4th), b. The isocenter location at the edge of irradiation field/penumbra region (beam 16th).

IMRT as shown in Fig. 11a. Whereas in Fig. 11b, gamma index evaluation only failed at high dose gradient and at the penumbra and umbra region.

All results for 2D planar dose evaluation using gamma index are presented in Tables 1 and 2. The results are summarized in Table 3. The acceptable gamma passing rate criteria for this study were set 95% for 4%/4 mm, 90% for 3%/3 mm and 85% for 2%, 2 mm. The sample data percentage which passed the acceptable criteria for non-split IMRT field were 83%, 94% and 89% and for split IMRT field were 36%, 68% and 32%, respectively, with the said criteria. These results show that almost all data for non-split IMRT field passed the acceptable criteria while almost all data for split IMRT field did not pass the acceptable criteria.

The data distribution for the gamma index passing rate can be seen in Figs. 12-14. The gamma pass-rate results for almost data with 2%/2 mm, 3%/3 mm and 4%/4 mm gamma criteria for non-split field were above 84%, 90% and 95%, while for split field were above 78%, 85% and 90%, respectively. The evaluation of split IMRT field was relatively poorer than non-split IMRT field and these were relevant with the evaluation of isocenter dose point. The reason that pixels at the junction of 2D dose reconstruction did not conform with the TPS calculation was

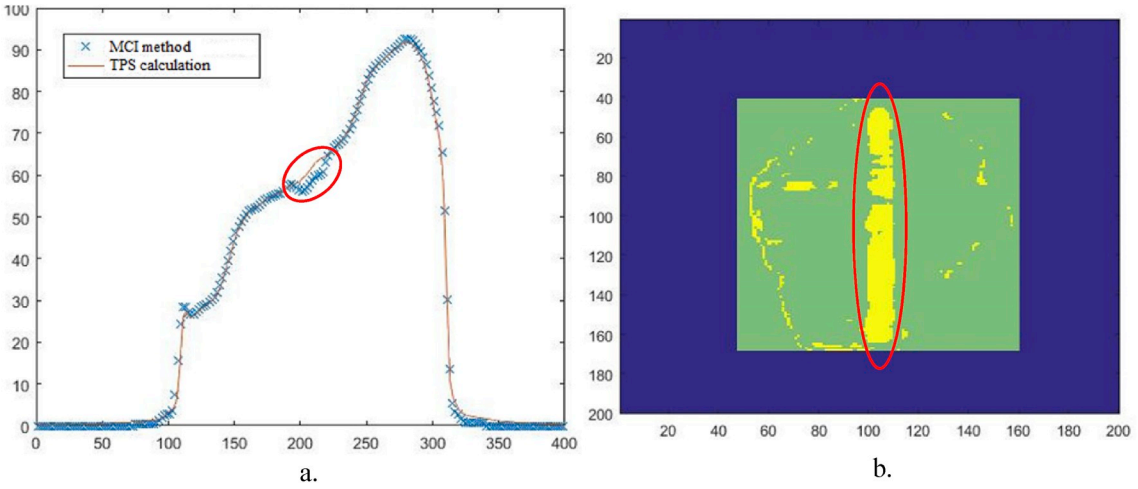

Fig. 10. a. Split IMRT field crossline profile between 2D dose reconstruction based on MCI method and TPS calculation, b. Image of gamma index evaluation of split IMRT field (3%,3 mm criteria). The red circles show the disagreement between the MCI method and TPS calculation at the junction where the IMRT beam is split. (For interpretation of the references to colour in this figure legend, the reader is referred to the Web version of this article.)

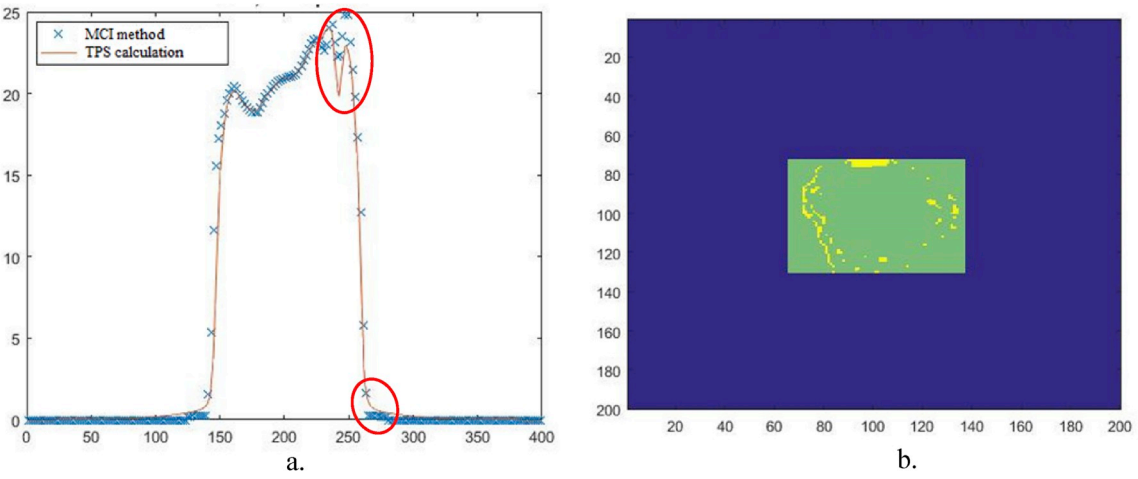

Fig. 11. a. Non-split IMRT field crossline profile between 2D dose reconstruction based on MCI method and TPS calculation, b. Image of gamma index evaluation of non-split IMRT field (3%,3 mm criteria). The red circles show the gamma index evaluation only failed at high dose gradient and at the penumbra and umbra region. (For interpretation of the references to colour in this figure legend, the reader is referred to the Web version of this article.)

Table 1
The results of gamma index evaluation between 2D dose reconstruction and TPS calculation for non-split IMRT field.

No	Location	Acceptable Gamma Passing Rate Criteria (%)					
		85% for 2%, 2 mm		90% for 3%, 3 mm		95% for 4%, 4 mm	
1	Brain 1	86.89	pass	94.65	pass	97.04	pass
2	Brain 1	90.24	pass	96.43	pass	98.58	pass
3	Brain 1	93.89	pass	98.16	pass	99.40	pass
4	Brain 1	90.57	pass	95.45	pass	97.13	pass
5	Brain 1	88.56	pass	94.94	pass	97.79	pass
6	Brain 2	90.21	pass	96.03	pass	98.41	pass
7	Brain 2	87.89	pass	96.02	pass	98.36	pass
8	Brain 2	89.96	pass	95.01	pass	97.27	pass
9	Brain 2	81.25	not pass	89.26	not pass	93.54	not pass
10	Brain 2	90.10	pass	95.04	pass	96.68	pass
11	Brain 2	90.38	pass	96.83	pass	98.68	pass
12	Left breast 1	85.49	pass	92.24	pass	95.82	pass
13	Left breast 1	85.20	pass	92.34	pass	95.61	pass
14	Left breast 1	84.22	not pass	92.04	pass	95.36	pass
15	Left breast 1	84.86	not pass	93.25	pass	96.20	pass
16	Left breast 1	86.72	pass	92.16	pass	94.62	not pass
17	Nasopharing	87.91	pass	94.62	pass	97.14	pass
18	Nasopharing	88.79	pass	93.73	pass	96.68	pass

because the dose reconstruction based on MU fluence had not been able to calculate accurately the dose within the edge of field and suspected. This was because the dose calculation only calculated the pixels that had non-zero value of MU fluence. To inspect this reason, it is needed to calculate the dose for all pixels MU fluence including for pixels that have zero value, but as the consequences, it will take a longer time to get the 2D dose distribution.

The gamma evaluation results show that the method to reconstruct 2D dose based on log files data in this study can be used for non-split IMRT field. Further research is required so the dose calculation can be more accurate to calculate the dose in the high dose gradient such as in the penumbra/umbra region. Further research to be more accurate to calculate the dose at the junction of split IMRT field is also required. The 2D dose reconstruction based on this study was relatively poorer than the dose reconstruction based on Mobius FX, because the gamma passing rate between the Mobius FX and TPS calculation for VMAT technique was above 98% for 2%, 2 mm gamma index criteria (Vazquez-Quino et al., 2017).

4. Conclusion

The isocenter dose evaluation results were 89% and 36% data for

Table 2
The results of gamma index evaluation between 2D dose reconstruction and TPS calculation for split IMRT field.

No	Location	Acceptable Gamma Passing Rate Criteria (%)					
		85% for 2%, 2 mm		90% for 3%, 3 mm		95% for 4%, 4 mm	
1	Right inguinal	85.45	pass	90.38	pass	93.73	not pass
2	Right inguinal	78.11	not pass	85.75	not pass	90.31	not pass
3	Right inguinal	82.54	not pass	90.05	pass	93.94	not pass
4	Right inguinal	83.59	not pass	88.91	not pass	92.93	not pass
5	Right inguinal	83.04	not pass	90.32	pass	94.69	not pass
6	Cervix	83.07	not pass	88.53	not pass	90.27	not pass
7	Cervix	67.13	not pass	90.03	pass	93.69	not pass
8	Cervix	78.42	not pass	90.64	pass	94.55	not pass
9	Cervix	83.89	not pass	89.86	not pass	93.87	not pass
10	Cervix	86.60	pass	94.94	pass	96.28	pass
11	Left breast 1	89.82	pass	95.41	pass	97.08	pass
12	Nasopharing	84.40	not pass	91.62	pass	95.10	pass
13	Nasopharing	88.50	pass	94.09	pass	96.66	pass
14	Nasopharing	84.17	not pass	90.60	pass	94.44	not pass
15	Nasopharing	80.88	not pass	88.52	not pass	92.78	not pass
16	Nasopharing	85.35	pass	91.63	pass	94.82	not pass
17	Left breast 2	85.49	pass	93.00	pass	96.16	pass
18	Left breast 2	84.88	not pass	91.58	pass	94.80	not pass
19	Left breast 2	80.31	not pass	87.15	not pass	91.18	not pass
20	Left breast 2	80.77	not pass	87.71	not pass	92.10	not pass
21	Left breast 2	88.30	pass	94.02	pass	96.88	pass
22	Left breast 2	85.52	pass	92.03	pass	95.44	pass

Table 3
The summary of the results of gamma index evaluation between 2D dose reconstruction and TPS calculation.

		Acceptable Gamma Passing Rate Criteria (%)		95% for 4%, 4 mm
		85% for 2%, 2 mm	90% for 3%, 3 mm	
non-split IMRT field	Pass criteria	15 data (83% from all data)	17 data (94% from all data)	16 data (89% from all data)
	didn't pass criteria	3 data (17% from all data)	1 data (6% from all data)	2 data (11% from all data)
split IMRT field	Pass criteria	8 data (36% from all data)	15 data (68% from all data)	7 data (32% from all data)
	didn't pass criteria	14 data (64% from all data)	7 data (32% from all data)	15 data (68% from all data)

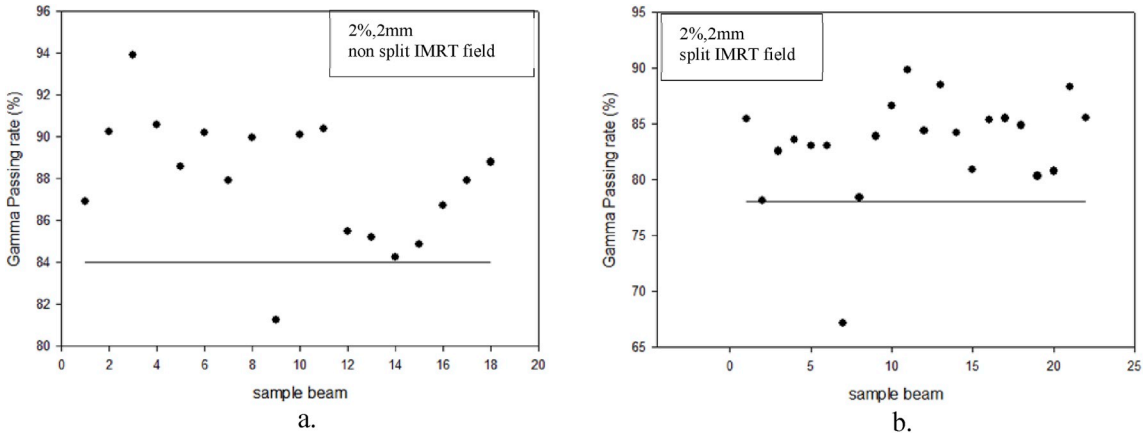

Fig. 12. The results of gamma evaluation 2%, 2 mm criteria between 2D dose reconstruction and TPS calculation a. Non-split IMRT field, b. Split IMRT field.

non-split field and split field had deviation under 3%. The gamma pass-rate results for non-split field with 2%/2 mm, 3%/3 mm and 4%/4 mm criteria were above 84%, 90% and 95%, respectively. On the other hand, the gamma pass-rate results for split field with 2%/2 mm, 3%/3 mm and 4%/4 mm criteria were above 78%, 85% and 90%, respectively. These results show that log file information can be used to reconstruct 2D dose distribution and potentially to be used for IMRT patient-specific QA. Further research is required, so the dose calculation can be more accurate to calculate the dose in the high dose gradient such as in the penumbra/umbra region and at the junction of split IMRT field.

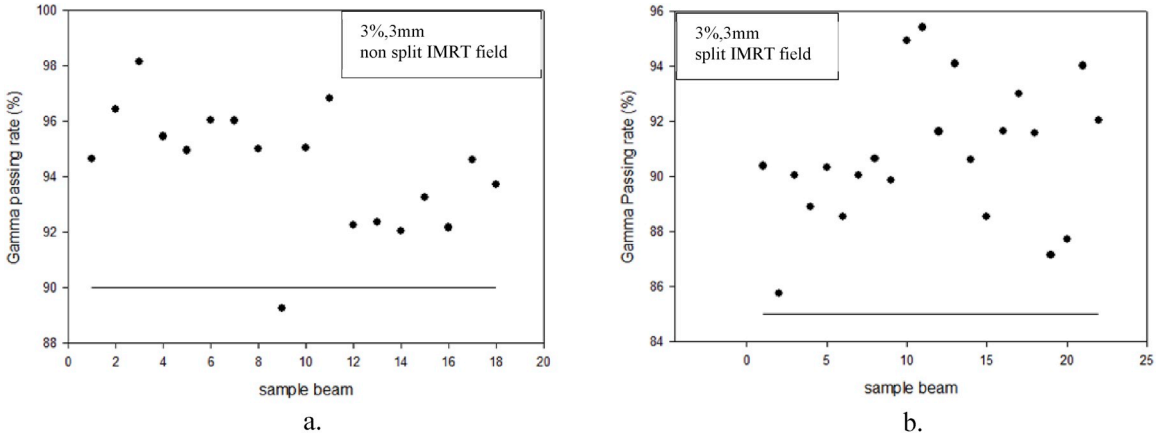

Fig. 13. The results of gamma evaluation 3%, 3 mm criteria between 2D dose reconstruction and TPS calculation a. Non-split IMRT field, b. Split IMRT field.

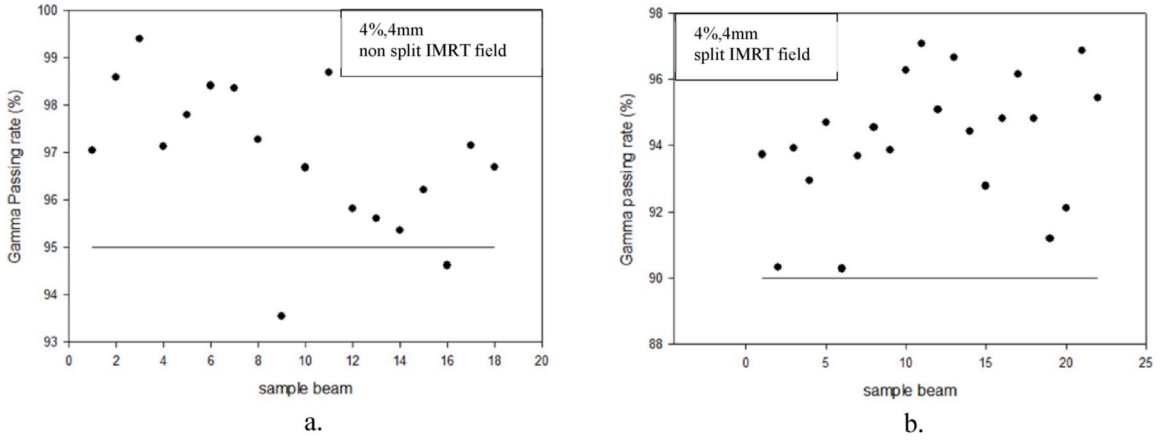

Fig. 14. The results of gamma evaluation 4%, 4 mm criteria between 2D dose reconstruction and TPS calculation a. Non-split IMRT field, b. Split IMRT field.

Acknowledgement

This study was supported by Universitas Indonesia Research Grant PIT9 with contract number NKB-0034/UN2.R3.1/HKP.05.00/2019

Appendix A. Supplementary data

Supplementary data to this article can be found online at https://doi.org/10.1016/j.radphyschem.2019.108473.

References

Biggs, P., D, P., Galvin, J., Sc, D., Klein, E., Sc, M., 2001. Basic applications, practical genetic algorithms. https://doi.org/10.1002/0471671746.ch4.

Chen, X., Yue, N.J., Chen, W., Saw, C.B., Heron, D.E., Stefanik, D., Antemann, R., Huq, M.S., 2005. A dose verification method using a monitor unit matrix for dynamic IMRT on Varian linear accelerators. Phys. Med. Biol. 50, 5641–5652. https://doi.org/10.1088/0031-9155/50/23/016.

DynaLog File Viewer Reference Guide, 2015. Varian Med. Syst. Inc..

Jeraj, M., Robar, V., 2004. Multileaf collimator in radiotherapy. Radiol. Oncol. 38, 235–240.

Jf, O., 2014. A Varian DynaLog file - based procedure for patient dose - volume histogram - based IMRT QA. J. Appl. Clin. Med. Phys. 15, 5–7. https://doi.org/10.1120/jacmp.v15i2.4665.A.

Khan, F.M., 2014. The Physics of Radiation Therapy. Lippincott Williams & Wilkins (LWW). Lippincott Williams & Wilkins. https://doi.org/10.1001/jama.1953.02940340098036.

Kung, J.H., Chen, G.T.Y., Kuchnir, F.K., 2000. A monitor unit verification calculation in intensity modulated radiotherapy as a dosimetry quality assurance. Med. Phys. 27, 2226–2230. https://doi.org/10.1118/1.1286553.

LoSasso, T., 2008. IMRT delivery performance with a varian multileaf collimator. Int. J. Radiat. Oncol. Biol. Phys. 71, 85–88. https://doi.org/10.1016/j.ijrobp.2007.06.082.

LoSasso, T., Chui, C.S., Ling, C.C., 1998. Physical and dosimetric aspects of a multileaf collimation system used in the dynamic mode for implementing intensity modulated radiotherapy. Med. Phys. 25, 1919–1927. https://doi.org/10.1118/1.598381.

McGarry, C.K., Agnew, C.E., Hussein, M., Tsang, Y., Hounsell, A.R., Clark, C.H., 2016. The use of log file analysis within VMAT audits. Br. J. Radiol. 89. https://doi.org/10.1259/bjr.20150489.

Midi, N.S., Zin, H.M., 2017. Feasibility of using the linac real-time log data for VMAT treatment verification. J. Phys. Conf. Ser. 851. https://doi.org/10.1088/1742-6596/851/1/012035.

Mubarok, S., Wibowo, W.E., Pawiro, S.A., 2019. Evaluation of MLC errors of LINAC based on log file. J. Phys. Conf. Ser. 1248. https://doi.org/10.1088/1742-6596/1248/1/012057.

Osewski, W., Dolla, Ł., Radwan, M., Szlag, M., Rutkowski, R., Smolińska, B., Ślosarek, K., 2014. Clinical examples of 3D dose distribution reconstruction, based on the actual MLC leaves movement, for dynamic treatment techniques. Rep. Pract. Oncol. Radiother. 19, 420–427. https://doi.org/10.1016/j.rpor.2014.04.013.

Rangaraj, D., Zhu, M., Yang, D., Palaniswaamy, G., Yaddanapudi, S., Wooten, O.H., Brame, S., Mutic, S., 2013. Catching errors with patient-specific pretreatment machine log file analysis. Pract. Radiation Oncology 3, 80–90. https://doi.org/10.1016/j.prro.2012.05.002.

Tae-Suk, S., Jeong-Woo, L., Jeong-Hoon, P., Jin-Beom, C., Ji-Yeon, P., Bo-Young, C., Doo-Hyun, L., Semie, H., Min-Young, K., Kyoung-Sik, C., 2009. Inverse verification of dose distribution for intensity modulated radiation therapy patient-specific quality assurance using dynamic MLC log files. J. Korean Phys. Soc. 55, 1649. https://doi.org/10.3938/jkps.55.1649.

Vazquez-Quino, L.A., Huerta-Hernandez, C.I., Rangaraj, D., 2017. Clinical experience with machine log file software for volumetric-modulated arc therapy techniques.

Baylor Univ. Med. Cent. Proc. 30, 276–279. https://doi.org/10.1080/08998280.2017.11929614.

Vial, P., Oliver, L., Greer, P.B., Baldock, C., 2006. An experimental investigation into the radiation field offset of a dynamic multileaf collimator. Phys. Med. Biol. 51, 5517–5538. https://doi.org/10.1088/0031-9155/51/21/009.

Xing, L., Chen, Y., Luxton, G., Li, J.G., Boyer, A.L., 2000. Monitor unit calculation for an intensity modulated photon field by a simple scatter-summation algorithm. Phys. Med. Biol. 45. https://doi.org/10.1088/0031-9155/45/3/401.

Yang, Y., Xing, L., Li, J.G., Palta, J., Chen, Y., Luxton, G., Boyer, A., 2003. Independent dosimetric calculation with inclusion of head scatter and MLC transmission for IMRT. Med. Phys. 30, 2937–2947. https://doi.org/10.1118/1.1617391.